NJC

PAPER

Synthesis and characterization of the nickel@carbon dots hybrid material and its application in the reduction of Cr(VI)†

Yali Guo, Dan Wang, Xiaoyu Liu, Xudong Wang, Weisheng Liu and Wenwu Qin*

The nickel@carbon dots hybrid material (Ni@C-dots) was prepared through a simple reduction route and characterized using transmission electron microscopy (TEM), X-ray diffraction (XRD), Fourier-transform infrared spectroscopy (FTIR), X-ray photoelectron spectroscopy (XPS) and fluorescence spectroscopy. Additionally, the hybrid material was tested as a catalyst to reduce toxic Cr(VI) to nontoxic Cr(III), and UV-vis spectrophotometry was employed to monitor the reduction process. According to the results, the Ni@C-dots hybrid material showed excellent hydrophilicity, good stability, and highly catalytic activity at room temperature.

1. Introduction

Carbon dots, a new type of photoluminescence (PL) carbon nanomaterial, were first obtained during the purification of single-walled carbon nanotubes in 2004.[1] In the past decade, carbon dots have attracted much interest because of the high photostability and lack of cytotoxicity, and C-dots have been reported to possess many significant applications, such as in bioimaging,[2–6] sensing,[7–10] photocatalysis, *etc*.[11–14]

Moreover, C-dots have also been used as an excellent support for nucleation and growth of the pristine nanocrystals due to the oxygen-containing functional groups on the surface.[15,16] On the other hand, metal nanoparticles (NPs) have emerged as a new class of materials and received considerable attention due to their unique electronic, optical, magnetic and catalytic properties.[17] However, few studies have been reported about metal nanoparticles supported on C-dots until now.[15,16,18,19] The combination of metal nanoparticles (Pd,[15,16] Ag,[16,18] Cu,[16] Au[19]) and C-dots provide a successful integration of the properties of the two components in the new hybrid materials.

To our knowledge, Cr(VI) is a leading contaminant in most hazardous waste sites and is also known to be a proven mutagen and a carcinogen. However, Cr(III) is believed to be an essential element to human metabolism.[20] Sadik *et al.* used colloidal palladium nanoparticles to rapidly catalyze the reduction of Cr(VI) to Cr(III).[20] Goutam *et al.* prepared an Ni–RGO composite

Key Laboratory of Nonferrous Metal Chemistry and Resources Utilization of Gansu Province and State Key Laboratory of Applied Organic Chemistry, College of Chemistry and Chemical Engineering, Lanzhou University, Lanzhou 730000, P. R. China. E-mail: qinww@lzu.edu.cn; Fax: +86-931-8912582; Tel: +86-931-8912582

as a catalyst to reduce Cr(VI).[21] A PdNP-supported mesoporous γ-Al$_2$O$_3$ film was also used as a catalyst for the reduction of Cr(VI).[22] In addition, nickel nanoparticles have been shown to have important applications in catalysts and magnetic materials.[23] Herein, we have prepared a novel Ni@C-dots hybrid material *via* a simple reduction route in the presence of C-dots and the hybrid material was tested as a catalyst to reduce Cr(VI) to Cr(III).

Fluorescence spectroscopy is an attractive technique that has proven to be a powerful research tool in many research fields, such as chemistry, biology and materials science.[24,25] Because most catalysts and substrates have no fluorescence (detectable signal), fluorescence spectroscopy has rarely been applied in the investigation of catalytic reactions. In principle, the intrinsic fluorescence of C-dots could be exploited to understand the photophysical properties of the catalyst and its catalytic mechanisms, which could aid the design of new catalysts.

2. Experimental section

2.1. Chemicals

Nickel(II) chloride (NiCl$_2$·6H$_2$O, Beijing Chemical Works, ≥98%), sodium borohydride (NaBH$_4$, Sinopharm Chem. Reagent Co., Ltd, ≥96%), citric acid monohydrate (CA, ≥99.5%), sodium hydroxide (NaOH, ≥96%), hydrazine monohydrate (H$_2$NNH$_2$·H$_2$O, ≥80%), formic acid (HCOOH, ≥98.5%) and ethylene glycol (HOCH$_2$CH$_2$OH) were purchased from Tianjin Guangfu Reagent Company. The other reagents used were potassium dichromate (K$_2$Cr$_2$O$_7$, Tianjin Chemical Reagent Research Institute, ≥99%), nickel(II) acetyl-acetonate (Ni(acac)$_2$, Tokyo Chemical Industry Co., Ltd, 99%), oleylamine, (Beijing J&K Reagent Company), trioctylphosphine (TOP, Chengdu Aceda Chem. Reagent Co., Ltd, 90%). All reagents

and solvents were of analytical grade and were directly used without further purification.

2.2. Instrument

Transmission electron microscopy (TEM) images were obtained on a JEM-2100 transmission electron microscope at an acceleration voltage of 120 kV. The samples were dispersed in ethanol and then dried on a holey carbon film Cu grid. Dynamic light scattering (DLS) was carried out on a BI-200SM (USA Brookhaven). XRD measurements were performed on a X-ray diffractometer (D/max-2400pc, Rigaku, Japan) using Cu Kα radiation (λ = 1.54178 Å), using an operating voltage and current of 40 kV and 60 mA, respectively. The 2θ range was from 10 to 80 in steps of 0.02°. For XRD observations, the samples were dispersed in aqueous solution and then dried on a glass slide. The Fourier transform infrared spectroscopy (FTIR) spectra were measured on a Nicolet 360 FTIR spectrometer using the KBr pellet technique. X-ray photoelectron spectra (XPS) were measured on a PHI-550 spectrometer by using Mg Kα radiation ($h\nu$ = 1253.6 eV) photo-emission spectroscopy with a base vacuum operated at 300 W.

2.3. Steady-state UV-vis absorption and fluorescence spectroscopy

The absorbance of the reduction process was recorded on a UV-visible spectrometer (Cary 100) at room temperature. The steady-state excitation and emission spectra were obtained on a FLS920 spectrofluorometer. Freshly prepared samples in 1 cm quartz cells were used to perform all UV-vis absorption and emission measurements.

2.4. Time-resolved fluorescence spectroscopy

Fluorescence lifetimes were measured on an Edinburgh Instruments FLS920 equipped with different light emitting diodes (excitation wavelength 330 nm and 360 nm), using the time-correlated single photon counting technique[26] in 2048 channels at room temperature. The sample concentrations were adjusted to optical densities at the excitation wavelength (330 or 360 nm) < 0.1. The monitored wavelengths were 440 nm, 450 nm, and 460 nm.

Histograms of the instrument response functions (using LUDOX scattering) and sample decays were recorded until they typically reached 5.0×10^3 counts in the peak channel. Obtained histograms were fitted as sums of the exponentials, using Gaussian-weighted nonlinear least squares fitting based on Marquardt–Levenberg minimization implemented in the software package of the instrument. The fitting parameters (decay times and preexponential factors) were determined by minimizing the reduced χ^2. An additional graphical method was used to judge the quality of the fit that included plots of surfaces ("carpets") of the weighted residuals vs. channel number. All curve fittings presented here had χ^2 values < 1.1. All measurements were done at 20 $^\circ$C.

2.5. Preparation of C-dots

C-dots were prepared according to a reported method.[27] Citric acid monohydrate (2 g) was heated hydrothermally in a Teflon-equipped stainless-steel autoclave at 200 $^\circ$C for 3 h. After cooling to room temperature, the orange syrup product was neutralized with NaOH solution (1 mol L^{-1}) and further dialyzed against double distilled water through a dialysis membrane (MWCO of 1 KDa).

2.6. Synthesis of Ni@C-dots

Typically, an amount of nickel chloride was dissolved directly in ethylene glycol, and 10 ml NiCl$_2$·6H$_2$O solution (45 mM) was mixed with 10 mL C-dots aqueous suspension in a 100 mL round bottom flask. Hydrazine hydrate (1.125 g) was then added to the mixture and maintained the concentration at 0.9 M. The mixture was kept vigorously stirring at 60 $^\circ$C for 10 min. Subsequently, 5 mg mL^{-1} NaBH$_4$ was added dropwise to initiate the reaction. The royal purple solution changed to dark which indicated the formation of Ni nanoparticles and was kept stirring for another 1 h at 60 $^\circ$C. The crude product was isolated through centrifugation and washed with absolute alcohol. After that, the pure product was dissolved in aqueous solution (5 mg mL^{-1}) to generate the colloidal suspension of Ni@C-dot nanoparticles.

2.7. Reduction of Cr(VI)

A UV-vis spectrophotometer was used to monitor the reduction process by observing the absorbance changes of the mixture between 300 and 500 nm. Typically, 10 mL of Cr(VI) (1 mM), 1 mL of formic acid (98.5%) and 9 mL of H$_2$O were added to a 50 mL beaker and the PH of the mixture was adjusted to 2.0. The absorption spectrum was recorded just after preparation of this solution, and 0.5 mL of colloidal Ni@C-dots nanoparticles were then added to the reaction mixture and absorption spectra were recorded at 2 min intervals. Similarly, the control experiments were also conducted.

3. Results and discussion

3.1. Characterization of C-dots and Ni@C-dots

The morphology and microstructure of the obtained C-dots and Ni@C-dots were characterized using TEM and dynamic light scattering (DLS). Fig. 1 demonstrates the morphology and the size of the prepared C-dots. The morphology of the prepared C-dots was regularly spherical with an average diameter about 5 nm. Dynamic light scattering (DLS) analysis also showed that the average hydrodynamic diameter of the C-dots was 4.4 nm (Fig. 1c).

The morphology of the Ni@C-dots hybrid material was different from that of C-dots. Fig. 2 shows the typical TEM images of the Ni@C-dots with core–shell nanostructures. They were formed with an ultrathin C-dot layer about 2 nm on the Ni nanoparticle (NP) surface. Each composite NP had a low contrast shell of continuous C-dot layers which were wrapped around a high contrast Ni core and indicated the formation of core–shell structures. Fig. 2c exhibits the HRTEM image of Ni@C-dots and it also demonstrates that the Ni cores are coated with ultrathin C-dot shells. The selected area electron
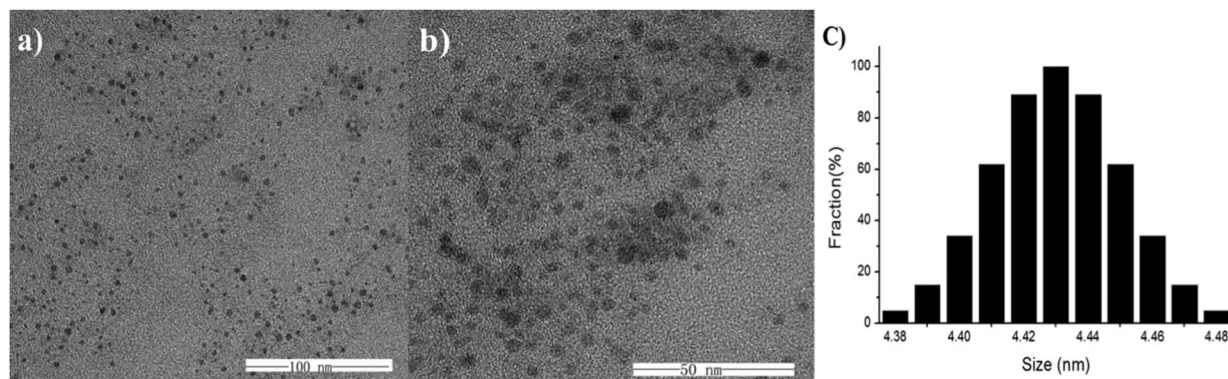
Fig. 1   (a, b) TEM images of C-dots with different magnifications. (c) Size distribution of C-dots.
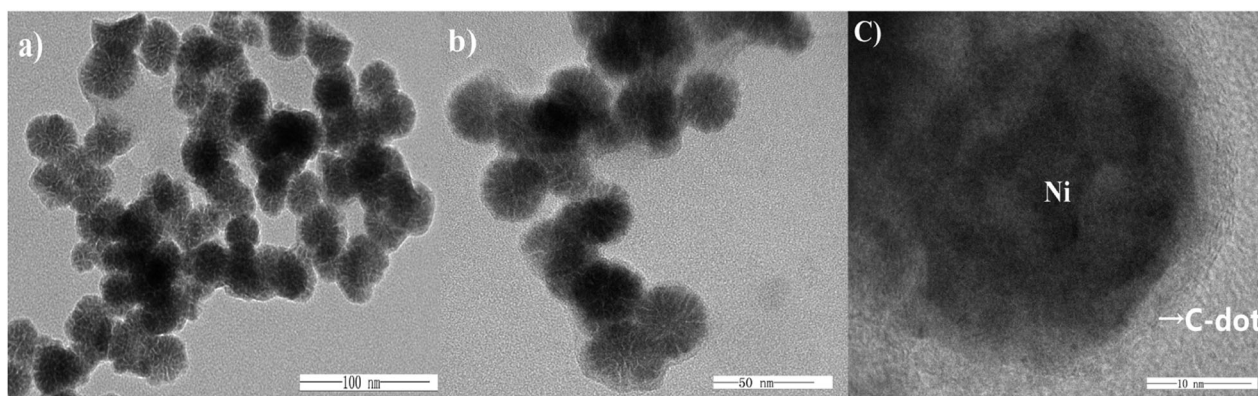

Fig. 2   (a, b) TEM images of Ni@C-dots with different magnifications. (c) HRTEM image of Ni@C-dot nanoparticles.

diffraction (SAED) pattern of Ni@C-dots displayed the diffraction rings assigned to the face-centered cubic (fcc) Ni(111) plane (Fig. S1†).

The powder XRD spectra of C-dots showed a broad peak centred at $2\theta = 23°$ (Fig. S2†), and Ni@C-dots showed a simple combination of an intense peak of C-dots at $2\theta = 23°$ and small peaks of fcc nickel ($2\theta = 44.5°$)[28] (Fig. 3).

Additionally, the FTIR spectra showed that the C-dots exhibited characteristic stretching vibrations of absorption bands of O–H at 3434 cm^{-1}, C=O at 1761 cm^{-1} and 1565 cm^{-1}. Notably, the C=O stretching peaks of the carbonyl at 1761 cm^{-1} disappeared when they were involved in NiNP formation, which might be attributed to the bonding interactions between the carboxylate groups and the metal (Fig. 4).[16]

In order to get further structural evidence, an XPS analysis of the Ni@C-dots was conducted (Fig. 5), and revealed three atom peaks at 289.5, 535.4 and 859.9 eV, which were attributed to C, O and Ni atoms, respectively.[29]
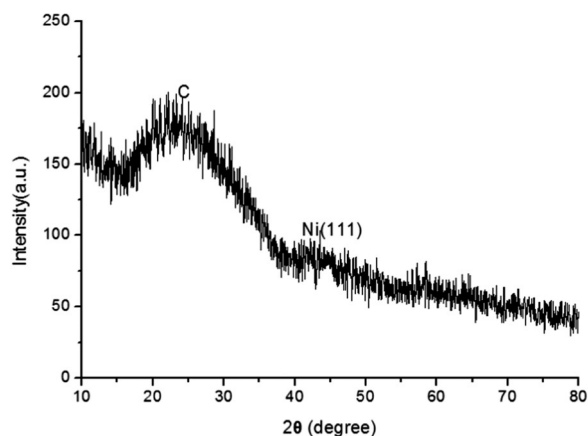

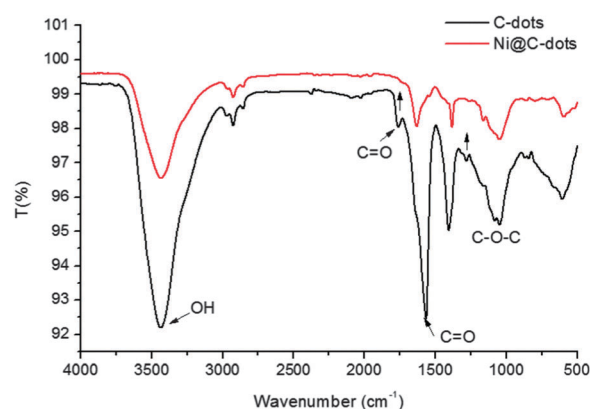Fig. 3   XRD spectra of Ni@C-dots deposited on a glass slide.

Fig. 4   FTIR spectra of C-dots and Ni@C-dots dried from an aqueous suspension using KBr pellets.
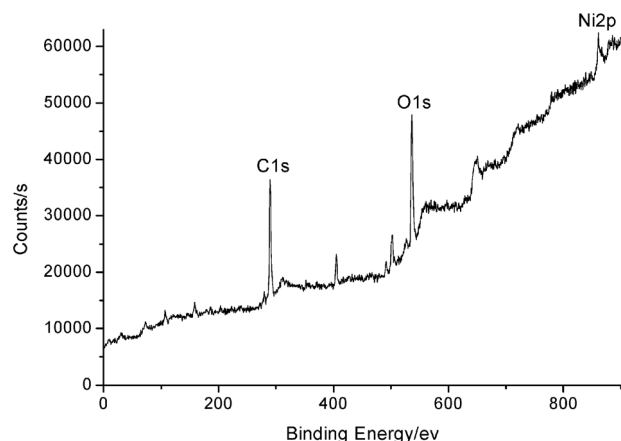
Fig. 5   XPS survey of the Ni@C-dots.

3.2.   Optical properties

The UV/Vis absorption spectra of C-dots dissolved in aqueous solution are depicted in Fig. 6a. The C-dots solution showed a broad UV/Vis absorption below 500 nm without any obvious peak, which is similar to that reported in the literature.[27] NiNPs had no ultraviolet absorption peak compared with Au, Ag or other metal nanoparticles. For example, Au and Ag NPs had a typical plasmon absorption peak at 543 nm[19] and 418 nm,[30] respectively. Hence, the UV/Vis absorption spectra of Ni@C-dots was similar to those of C-dots (Fig. 6a).

To further explore the optical properties of the prepared C-dots, a detailed photoluminescence study was carried out by using different excitation wavelengths (Fig. 6b), and the results showed that the corresponding emissions of the C-dots covered the wavelength range from blue to green. The most intense PL of the C-dots dispersion appeared at 449 nm upon excitation at 340 nm. The emission bands shifted with the increasing excitation wavelength, which revealed a distribution of the different surface energy traps toward the C-dots.[31,32] The fluorescence emission intensity of C-dots decreased following the increased excitation wavelength (longer than 340 nm). Recently, we had reported the photoluminescence properties of Ni@SiO₂–C-dots magnetic nanocomposite not only in solution but also in the solid state.[29] In this contribution, Ni@C-dots showed excellent hydrophilicity compared to the Ni@SiO₂–C-dots magnetic nanocomposite. The photophysical properties of Ni@C-dots in water were quite different when compared with that of the Ni@SiO₂–C-dots magnetic nanocomposite. The PL emission spectra and photoluminescence intensity of the Ni@SiO₂–C-dots magnetic nanocomposite in ethanol could be observed by the change of the excitation wavelength. In contrast, the formation of Ni@C-dots here partly quenched the PL of C-dots as shown in Fig. 6c. It was demonstrated that photoexcited C-dots could serve as both electron donors and electron acceptors and their photoluminescence could be quenched efficiently by either electron acceptor or donor molecules.[33] The photoinduced electron was transferred from C-dot shells to Ni cores or from Ni cores to C-dot shells. Thus the formation of Ni@C-dots partly quenched the photoluminescence of C-dots.
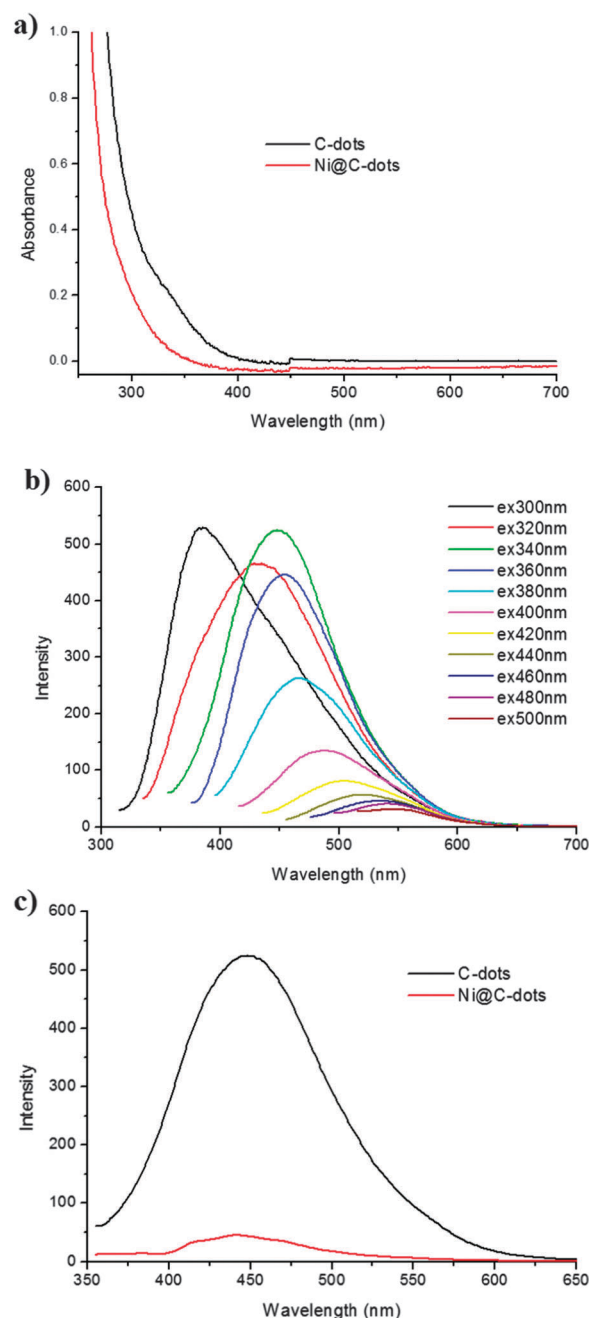

Fig. 6   (a) UV-visible absorption spectrum of C-dots and Ni@C-dots aqueous suspension. (b) PL spectra of C-dots aqueous suspension upon excitation at different excitation wavelengths. (c) PL spectrum of C-dots and Ni@C-dots aqueous suspension excited at 340 nm.

To investigate the fluorescence dynamics of C-dots and Ni@C-dots, fluorescence decay traces for the C-dots and Ni@C-dots in aqueous solution were collected as a function of emission wavelength λ_{em} through the single-photon timing technique. (Fig. 7, Table 1 and Fig. S3–S5†). Each fluorescence decay trace was analyzed individually as a sum of two exponential function in terms of decay times τ_i and associated bi-exponential factors τ_i. Table 1 summarized the time resolved fluorescence data of C-dots and Ni@C-dots in aqueous solution.
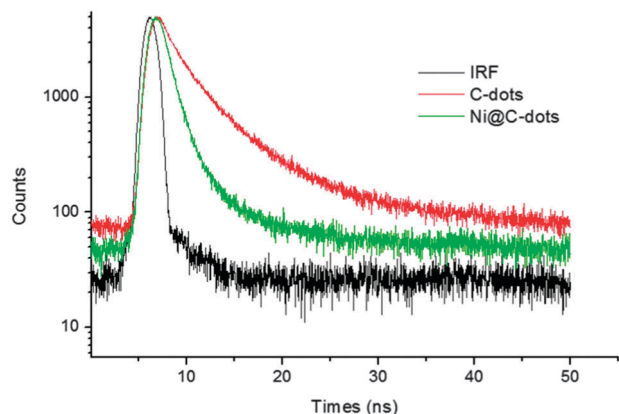
Fig. 7 Fluorescence decay profiles (λ_{ex} = 330 nm and λ_{em} = 450 nm) of C-dots and Ni@C-dots aqueous suspension.

Table 1 Photophysical properties of C-dots and Ni@C-dots aqueous suspension. Decay times τ_1, τ_2 and the relative amplitude (%)

Compound	Excitation wavelength/ nm	Monitored emission wavelength/ nm	τ_1/ns	τ_2/ns
C-dots	330	440	1.52 (40.83%)	5.21 (59.17%)
		450	1.56 (39.49%)	5.27 (60.51%)
		460	1.61 (38.00%)	5.39 (62.00%)
	360	440	1.54 (38.29%)	4.93 (64.71%)
		450	1.51 (37.50%)	4.95 (62.50%)
		460	1.61 (37.82%)	5.07 (62.18%)
Ni@C-dots	330	440	1.03 (87.80%)	3.95 (12.20%)
		450	1.07 (87.39%)	4.99 (12.61%)
		460	1.07 (87.36%)	5.11 (12.64%)
	360	440	1.05 (86.08%)	2.54 (13.92%)
		450	1.07 (86.80%)	2.57 (13.20%)
		460	1.09 (89.74%)	3.16 (10.26%)

Before an attempt is made to analyze the results, it is worth recapitulating the literature data on C-dots and Ni@SiO$_2$–C-dots magnetic nanocomposite. For C-dots in ethanol, a tri-exponential function ($\sim$1.0 ns, $\sim$5.0 ns and $\sim$13.0 ns) was used to fit the decay at all three emission wavelengths. The fluorescence decay of the Ni@SiO$_2$–C-dots nanocomposite powder in the solid state at λ_{ex} = 330 or 360 nm can be described as a bi-exponential function with the contributions of the τ_1 ($\sim$3.0 ns) and τ_2 ($\sim$9.0 ns) components, respectively. In ethanol, at the excitation of λ_{ex} = 330 or 360 nm, the fluorescence decays for Ni@SiO$_2$–C-dots magnetic clearly showed tri-exponential behaviour ($\sim$1.0 ns, $\sim$5.0 ns and $\sim$11.0 ns).[29] As we have mentioned before, because the C-dots and Ni@C-dots were not the same as those reported in the literature, the photophysical properties of Ni@C-dots in water were quite different when compared with those of the Ni@SiO$_2$–C-dots magnetic nanocomposite. The fluorescence decay of C-dots in this article was fitted to the bi-exponential profile (λ_{ex} = 330 nm), and the fast component τ_1 ($\sim$1.6 ns) had an amplitude of about 39%, whereas the contribution of the τ_2 ($\sim$5.3 ns) component was about 61%. The different emission wavelengths of C-dots did not induce an obvious change in the fluorescence decay. The third

lifetime could not be determined, which might be because it had an almost negligible contribution corresponding to the decay time. The fluorescence decay for Ni@C-dots also revealed a bi-exponential profile, and the longer lifetime decreased ($\sim$5.3 to $\sim$2.5 ns) along with a decrease in the amplitude ($\sim$61% to $\sim$13%). The shorter component remained almost constant ($\sim$1.6 to $\sim$1.1 ns), and the contribution of this component increased ($\sim$39% to $\sim$87%). For the decay traces displayed in Fig. 7, it was clear that the fluorescence lifetimes of Ni@C-dots decreased (become shorter) when compared with that of C-dots. The observation of this decreasing fluorescence lifetime for Ni@C-dots was in line with its lower fluorescence intensity compared to that of C-dots. The difference in the steady-state and time-resolved fluorescence spectrum properties between Ni@C-dots and C-dots indicated the formation of the Ni@C-dots hybrid material.

3.3. Catalytic properties

The reduction of Cr(VI) using Ni@C-dots catalyzed formic acid was monitored by using a UV-visible absorption spectrometer. The result displayed the changes in the intensity of the absorption peak of $Cr_2O_7^{2-}$ at 350 nm. After a 10 min reaction, the adsorption peak of Cr(VI) nearly disappeared and the color of the solution changed from yellow to colorless in the presence of Ni@C-dots, confirming the complete reduction of Cr(VI) to Cr(III) (Fig. 8b).[21] The presence of Cr(III) in the colorless solution was confirmed by treating it with excess NaOH solution upon which the solution turned green due to the formation of hexahydroxochromate(III).[22] However, the blank experiment without the Ni@C-dots did not show any changes in the color or adsorption peak of Cr(VI), which further proved the catalytic activity of Ni@C-dots (Fig. 8a). Control experiments for this reaction were also performed in the presence of bare Ni NPs[28] or pure C-dots under standard experimental conditions (S1.2.1–S1.2.2, Fig. S7 and S8†). Fig. 9 shows the relationship between the concentration ratio (C/C_0) of Cr(VI) and the reaction time for different catalysts. The reduction rate was apparently slower in the presence of bare Ni NPs than that of the Ni@C-dots hybrid material. On the other hand, C-dots did not show any catalytic activity towards Cr(VI) reduction. The above results indicate that Ni@C-dots exhibit higher catalytic activity and faster reduction rate than NiNPs or C-dots. It is worth noting that all of catalytic reduction experiments were performed at pH = 2.0, and the optimal pH had been previously proposed for a more effective reduction of Cr(VI) to Cr(III).[34] $Cr_2O_7^{2-}$ was converted into CrO_4^{2-} at higher PH and the UV-visible peak position of $Cr_2O_7^{2-}$ shifted toward higher wavelength with time due to the formation of CrO_4^{2-} ions.[21]

On the basis of the experiment results, a plausible mechanism for this redox reaction was proposed. Initially, HCOOH was adsorbed on the surface of Ni@C-dots and a redox reaction occurred between Ni NPs and HCOOH on the C-dots surface. Then HCOOH decomposed to give CO$_2$ and hydrogen (H$^\bullet$). Subsequently, the free hydrogen atom reduced the Cr(VI) species to the Cr(III) species. Fig. S6† shows that the morphology of the prepared bare Ni NPs was monodisperse and regularly spherical, and the morphology of the Ni@C-dots hybrid material was
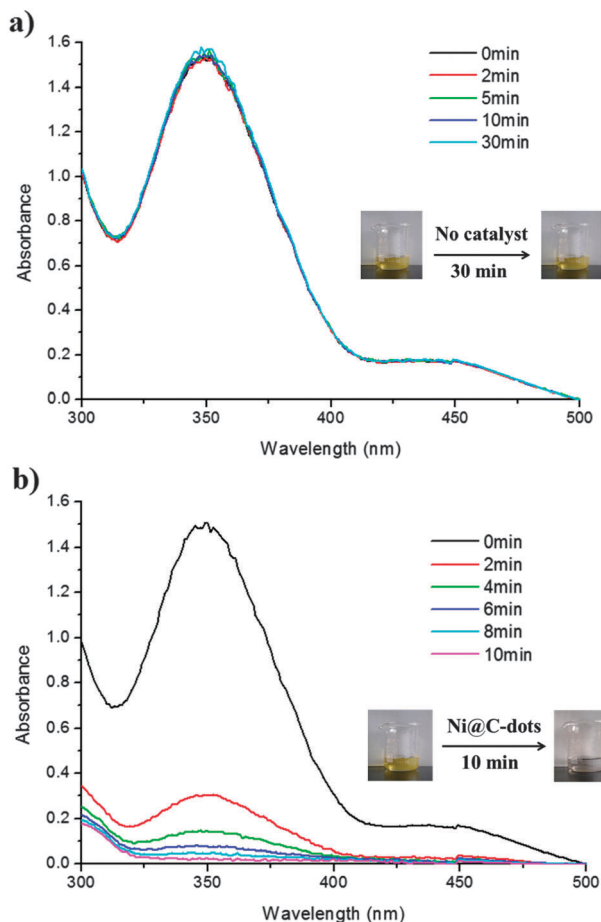
Fig. 8 UV-visible spectral evolution with time during the reduction of Cr(VI) by formic acid at room temperature in the absence (a) and in the presence (b) of Ni@C-dots. Insets are visible color changes of Cr(VI) under daylight.
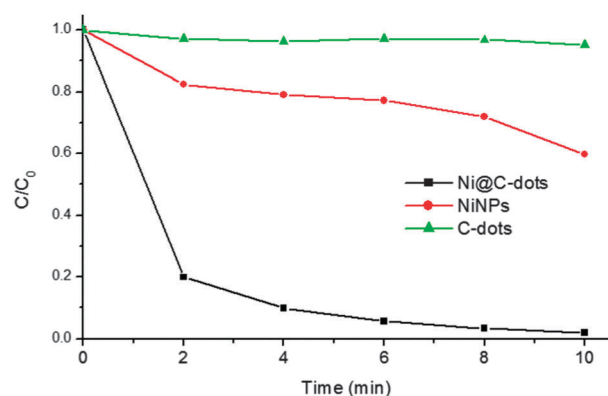

Fig. 9 The relationship between concentration ratio (C/C_0) of Cr(VI) and reaction time for different catalysts.

Table 2 Photophysical properties of Ni@C-dots after catalytic reduction of Cr(VI). Decay times τ_1, τ_2 and the relative amplitude (%)

Compound	Excitation wavelength/ nm	Monitored emission wavelength/ nm	τ_1/ns	τ_2/ns
Ni@C-dots	330	440	0.87 (91.52%)	3.47 (8.48%)
		450	0.88 (89.74%)	3.59 (10.26%)
		460	0.87 (89.34%)	3.74 (10.66%)
	360	440	0.85 (89.79%)	2.93 (10.21%)
		450	0.86 (88.30%)	3.10 (11.70%)
		460	0.83 (86.70%)	2.94 (13.30%)

room temperature. For bare Ni NPs, there was no electronic transmission medium to accelerate the electron transfer. Hence, the rate of the reduction reaction dropped to a lower level compared to that for the Ni@C-dots.

In order to study the stability of the catalyst, we studied the time resolved fluorescence and XPS to the catalyst after the catalytic reaction. Table 2 showed the time resolved fluorescence data of Ni@C-dots after the catalytic reduction of Cr(VI).

Compared with the data obtained before catalytic reduction (Table 1), the time resolved fluorescence data of Ni@C-dots after the reaction remained nearly constant when the errors were taken into account. It indicated that Ni@C-dots hybrid material was steady and did not take part in the reaction process. In order to get further information about the chemical state of Ni in the Ni@C-dots before and after the catalytic reaction, we performed high resolution XPS analysis as shown in Fig. 10. HRXPS of Ni in Ni@C-dots before reduction revealed the peaks at 855.8 and 873.7 eV corresponding to $2p_{3/2}$ and $2p_{1/2}$, respectively. After reduction of Cr(VI), the peaks of Ni$2p_{3/2}$ and Ni$2p_{1/2}$ shifted to 856.9 and 875.1 eV, respectively. Compared to the data before reduction of Cr(VI), the HRXPS data of Ni nearly remained constant when the errors were taken into account, which suggested the stability and minimal structural changes of Ni nanoparticles during the catalytic reaction.
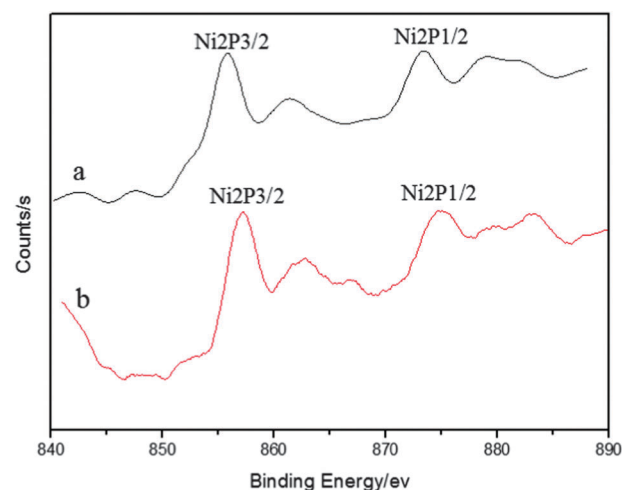

Fig. 10 HRXPS spectra of Ni in Ni@C-dots (a) before (b) and after reduction of Cr(VI).

different from that of the bare Ni NPs. The Ni@C-dots hybrid material was core–shell nanostructured and it was formed with an ultrathin C-dot layer around the Ni NP surface (Fig. 2). It is noteworthy that the reduction step involved an electron-transfer process[21] and C-dots with excellent electron transfer property[35] could transfer the electron rapidly to reduce Cr(VI) at

4. Conclusions

In summary, we have successfully prepared the Ni@C-dots hybrid material with ultrathin carbon dots shells of size about 2 nm. The HRTEM clearly revealed the C-dot shells and Ni cores. The C-dots served as an excellent support for nucleation to grow nanoparticles and to prevent agglomeration. The morphology, structure and optical properties of the hybrid material were studied. Further catalytic experiments suggested that Ni@C-dots exhibited high catalytic activity towards the reduction of Cr(VI) to Cr(III) by using formic acid as the reducing agent under room temperature. Our studies provide an approach to design novel functional composites and an effective catalyst to govern water pollution.

Acknowledgements

Notes and references

1 X. Y. Xu, R. Ray, Y. L. Gu, H. J. Ploehn, L. Gearheart, K. Raker and W. A. Scrivens, *J. Am. Chem. Soc.*, 2004, **126**, 12736–12737.

2 L. Cao, X. Wang, M. J. Meziani, F. S. Lu, H. F. Wang, P. G. Luo, Y. Lin, B. A. Harruff, L. M. Veca, D. Murray, S. Y. Xie and Y. P. Sun, *J. Am. Chem. Soc.*, 2007, **129**, 11318–11319.

3 R. Liu, D. Wu, S. Liu, K. Koynov, W. Knoll and Q. Li, *Angew. Chem., Int. Ed.*, 2009, **48**, 4598–4601.

4 F. Wang, Z. Xie, H. Zhang, C. Y. Liu and Y. G. Zhang, *Adv. Funct. Mater.*, 2011, **21**, 1027–1031.

5 S. C. Ray, A. Saha, N. R. Jana and R. Sarkar, *J. Phys. Chem. C*, 2009, **113**, 18546–18551.

6 S. J. Zhu, J. H. Zhang, C. Y. Qiao, S. J. Tang, Y. F. Li, W. J. Yuan, B. Li, L. Tian, F. Liu, R. Hu, H. N. Gao, H. T. Wei, H. Zhang, H. C. Sun and B. Yang, *Chem. Commun.*, 2011, **47**, 6858–6860.

7 H. X. Zhao, L. Q. Liu, Z. D. Liu, Y. Wang, X. J. Zhao and C. Z. Huang, *Chem. Commun.*, 2011, **47**, 2604–2606.

8 W. L. Wei, C. Xu, J. S. Ren, B. L. Xu and X. G. Qu, *Chem. Commun.*, 2012, **48**, 1284–1286.

9 L. Zhou, Y. H. Lin, Z. Z. Huang, J. S. Ren and X. G. Qu, *Chem. Commun.*, 2012, **48**, 1147–1149.

10 S. Liu, J. Q. Tian, L. Wang, Y. W. Zhang, X. Y. Qin, Y. L. Luo, A. M. Asiri, A. O. Al-Youbi and X. P. Sun, *Adv. Mater.*, 2012, **24**, 2037–2041.

11 H. T. Li, X. D. He, Z. H. Kang, Y. Liu, J. L. Liu, S. Y. Lian, C. H. A. Tsang, X. B. Yang and S.-T. Lee, *Angew. Chem., Int. Ed.*, 2010, **49**, 4430–4434.

12 L. Cao, S. Sahu, P. Anilkumar, C. E. Bunker, J. Xu, K. A. S. Fernando, P. Wang, E. A. Guliants, K. N. Tackett and Y. P. Sun, *J. Am. Chem. Soc.*, 2011, **133**, 4754–4757.

13 B. Y. Yu and S. Y. Kwak, *J. Mater. Chem.*, 2012, **22**, 8345–9353.

14 Z. Ma, H. Ming, H. Huang, Y. Liu and Z. H. Kang, *New J. Chem.*, 2012, **36**, 861–864.

15 D. Dey, T. Bhattacharya, B. Majumdar, S. Mandani, B. Sharma and T. K. Sarma, *Dalton Trans.*, 2013, **42**, 13821–13825.

16 L. Tian, D. Ghosh, W. Chen, S. Pradhan, X. J. Chang and S. W. Chen, *Chem. Mater.*, 2009, **21**, 2803–2809.

17 P. D. Cozzoli, T. Pellegrino and L. Manna, *Chem. Soc. Rev.*, 2006, **35**, 1195–1208.

18 L. M. Shen, M. L. Chen, L. L. Hu, X. W. Chen and J. H. Wang, *Langmuir*, 2013, **29**, 16135–16140.

19 P. H. Luo, C. Li and G. Q. Shi, *Phys. Chem. Chem. Phys.*, 2012, **14**, 7360–7366.

20 M. A. Omole, I. O. K'Owino and O. A. Sadik, *Appl. Catal., B*, 2007, **76**, 158–167.

21 K. Bhowmik, A. Mukherjee, M. K. Mishra and G. De, *Langmuir*, 2014, **30**, 3209–3216.

22 A. Dandapat, D. Jana and G. De, *Appl. Catal., A*, 2011, **396**, 34–39.

23 S.-H. Wu and D.-H. Chen, *J. Colloid Interface Sci.*, 2003, **259**, 282–286.

24 F. V. Bright, *Anal. Chem.*, 1988, **60**, 1031A–1039A.

25 A. Tcherniak, C. Reznik, S. Link and C. F. Landes, *Anal. Chem.*, 2009, **81**, 746–754.

26 N. Boens, W. W. Qin, N. Basaric, J. Hofkens and M. Ameloot, *Anal. Chem.*, 2007, **79**, 2137–2149.

27 Y. Q. Dong, H. C. Pang, H. B. Yang, C. X. Guo, J. W. Shao, Y. W. Chi, C. M. Li and T. Yu, *Angew. Chem., Int. Ed.*, 2013, **52**, 7800–7804.

28 J. C. Park, H. J. Lee, J. U. Bang, K. H. Park and H. J. Song, *Chem. Commun.*, 2009, 7345–7347.

29 D. Wang, Y. L. Guo, W. S. Liu and W. W. Qin, *RSC Adv.*, 2014, **4**, 7435–7439.

30 P. Raveendran, J. Fu and S. L. Wallen, *Green Chem.*, 2006, **8**, 34–38.

31 X. F. Jia, J. Li and E. K. Wang, *Nanoscale*, 2012, **4**, 5572–5575.

32 Z. Lin, W. Xue, H. Chen and J. M. Lin, *Anal. Chem.*, 2011, **83**, 8245–8251.

33 X. Wang, L. Cao, F. S. Lu, M. J. Meziani, H. T. Li, G. Qi, B. Zhou, B. A. Harrufff, F. Kermarrec and Y.-P. Sun, *Chem. Commun.*, 2009, 3774–3776.

34 F. Jiang, Z. Zheng, Z. Y. Xu, S. R. Zheng, Z. B. Guo and L. Q. Chen, *J. Hazard. Mater.*, 2006, **134**, 94–103.

35 H. T. Li, Z. H. Kang, Y. Liu and S.-T. Lee, *J. Mater. Chem.*, 2012, **22**, 24230–24253.